Biophysical Reports

ARTICLE

Probing DNA-protein interactions using single-molecule diffusivity contrast

Hugh Wilson,[1] Miles Lee,[1] and Quan Wang[1,*]
[1]Lewis-Sigler Institute for Integrative Genomics, Princeton University, Princeton, New Jersey

ABSTRACT Single-molecule fluorescence investigations of protein-nucleic acid interactions require robust means to identify the binding state of individual substrate molecules in real time. Here, we show that diffusivity contrast, widely used in fluorescence correlation spectroscopy at the ensemble level and in single-particle tracking on individual (but slowly diffusing) species, can be used as a general readout to determine the binding state of single DNA molecules with unlabeled proteins in solution. We first describe the technical basis of drift-free single-molecule diffusivity measurements in an anti-Brownian electrokinetic trap. We then cross-validate our method with protein-induced fluorescence enhancement, a popular technique to detect protein binding on nucleic acid substrates with single-molecule sensitivity. We extend an existing hydrodynamic modeling framework to link measured diffusivity to particular DNA-protein structures and obtain good agreement between the measured and predicted diffusivity values. Finally, we show that combining diffusivity contrast with protein-induced fluorescence enhancement allows simultaneous mapping of binding stoichiometry and location on individual DNA-protein complexes, potentially enhancing single-molecule views of relevant biophysical processes.

WHY IT MATTERS The interactions between proteins and nucleic acids (DNA and RNA) are fundamental to many aspects of life. Single-molecule observations of these processes can provide key insights at the molecular level. In these experiments, it is important to robustly identify the binding state of the nucleic acid substrate. Using single-molecule diffusometry, we show the translational diffusion coefficient can be used as a general contrast mechanism to differentiate protein-bound and free DNA at the single-molecule level. We validate our approach using DNA-restriction enzyme systems and demonstrate simultaneous mapping of the binding stoichiometry and position of two proteins on the same DNA substrate. Our method could enable direct single-molecule views of many biophysical processes in protein-nucleic acid interactions.

INTRODUCTION

Single-molecule fluorescence measurements of protein-nucleic acid interactions have revealed new insights into the maintenance and processing of genomic information (see recent reviews (1–7) and the references therein). In these experiments, access to the binding state of individual substrate molecules is essential and can be measured by labeling both the substrate and the protein with different reporters to look for colocalization (8,9) or a Förster resonance energy transfer (10,11) signal. However, the requirement to fluorescently tag the protein, often at site-specific locations, complicates the experimental design and limits the maximal allowable protein concentration because of background fluorescence (12,13) (e.g., ∼10 nM for total internal reflection microscopy).

Recently, protein-induced fluorescence enhancement (PIFE) has been developed as a powerful alternative to detect protein-nucleic acid binding without labeling the protein (14–16). In the PIFE assay, a fluorescent probe on the DNA (or RNA) becomes brighter when an unlabeled protein binds in its vicinity, and the degree of fluorescence enhancement depends on the dye-protein distance within a range of ∼0–3 nm. This phenomenon is generally understood as leveraging the unique photophysical properties of cyanine dyes (e.g., Cy3, Cy5, and DY547): the binding of a nearby protein suppresses the otherwise efficient, nonradiative photoisomerization pathway from the dye's singlet excited state, likely because of steric

Submitted May 19, 2021, and accepted for publication July 20, 2021.
*Correspondence: quanw@princeton.edu
Editor: Yoav Shechtman.
https://doi.org/10.1016/j.bpr.2021.100009

hindrance (17). Because PIFE elegantly bypasses the requirement for protein labeling, it has gained popularity in recent years in many single-molecule studies of protein-nucleic acid systems (14,18–22).

In this work, we aim to develop an alternative contrast mechanism to probe protein-nucleic acid interactions, using the physical properties of single molecules, without protein labeling. Measurements of hydrodynamic properties report on the global size and shape of macromolecules and are widely used to characterize biomolecular interactions at the ensemble (23,24) and subensemble (25) levels. In addition, single-particle tracking (26) is frequently used to detect interactions of individual biomolecules when diffusion is slow ($D < 10\ \mu m^2/s$), for example in membrane-bound (27) or viscous cellular contexts (28,29). Previously, we developed a diffusometry platform based on an Anti-Brownian ELectrokinetic (ABEL) trap (30) (Materials and methods) that is capable of precisely measuring the translational diffusion coefficient (D) of individual, fast-diffusing biomolecules ($D \sim 100\ \mu m^2/s$) in solution. Leveraging this advance, we reasoned that D would be a direct physical parameter to sense protein-nucleic acid interactions at the single-molecule level. In this work, we demonstrate this modality and cross-validate with PIFE (Fig. 1). To link measured diffusivity values to particular molecular complexes, we extend the "HullRad" framework (31) to model the diffusion coefficient of DNA-protein complexes that could be present in experiments. Further, we demonstrate the unique capability to independently resolve protein binding stoichiometry and binding location on a single short DNA molecule by combining diffusivity contrast with PIFE.

MATERIALS AND METHODS

Sample preparation

DNA samples were ordered from Integrated DNA Technologies (Coralville, IA) and used without further purification. Detailed construct, information including sequences and dye labeling positions, can be found in Table S1. Duplexes were formed by mixing the labeled and the complementary strands with a ratio of 1:1.5 in HN100 buffer (20 mM HEPES (pH 8.0) and 100 mM NaCl), heating to 90°C for 2 min, and gradually cooling to room temperature (over 30–60 min). Restriction enzymes (*Bam*HI and *Eco*RI) were purchased from New England BioLabs (Ipswich, MA) (*Bam*HI: R0136M, *Eco*RI: R0101M) and used without further purification. The stock concentrations of the enzymes (*Bam*HI: 1.1 μM, *Eco*RI: 0.74 μM) were provided by New England BioLabs. ABEL trap experiments were performed in a buffer containing 20 mM HEPES (pH 7.8), 25 mM NaCl, 2 mM $CaCl_2$ with 5–10 pM labeled DNA duplex, 1–10 nM *Bam*HI, and/or 0.4–5 nM *Eco*RI. An oxygen scavenger system [50 or 100 nM protocatechuate 3,4-dioxygenase (OYC Americas, Vista, CA) and 2 mM protocatechuic acid (Sigma, St. Louis, MO)] and 2 mM Trolox were added to suppress Cy5 blinking and photobleaching (32). The final sample solution also contained ~0.5 pM Atto647N-labeled single-stranded DNA (5′-Atto647N-AAC TTG ACC C), which served as a fiducial marker of diffusion coefficient measurement consistency across different experimental runs.

ABEL trap implementation

The ABEL trap was implemented similarly to previously published designs (30,33) using an RM21 microscope frame (Mad City Labs, Madison, WI). Briefly, we implemented a rapid, acousto-optic laser scanning and photon-by-photon mapping scheme to detect the position of a fast-diffusing single molecule in solution. The detected molecule positions were refined by a hardware-coded (NI, PCIe7852R) Kalman filter (34) before being used to compute the feedback voltages for

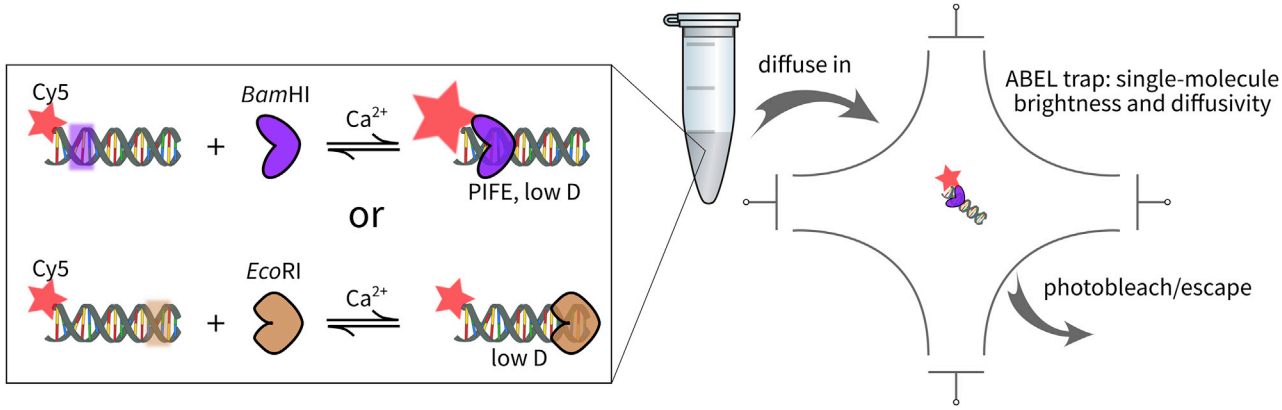

FIGURE 1 Probing DNA-protein interactions by single-molecule diffusivity contrast. The binding between short duplex DNA molecules (15–52 bp in length) and two restriction enzymes is used to validate the method (*left box*). For each DNA length, there is a *Bam*HI binding site (*purple shaded box*) 2 bp away from the terminal Cy5 label. Binding of *Bam*HI is expected to simultaneously enhance the brightness of Cy5 (via protein-induced fluorescence enhancement, PIFE) and lower the diffusion coefficient. Some DNA molecules also have an *Eco*RI binding site (*brown shaded box*) far from the Cy5 label, and only a diffusivity change, not PIFE, is expected upon *Eco*RI binding. The experiments are conducted by loading a sample containing labeled DNA (~pM concentration) and restriction enzyme (~nM concentration) into an ABEL trap microfluidic device (*right schematic*). Individual molecules are captured by feedback electrokinetic trapping, and their brightness and diffusivity are determined.

molecule trapping. With minimal delay (~μs), these voltages were amplified and applied to a microfluidic sample chamber to counteract Brownian motion in two dimensions (x and y). The motion of the molecule in the longitudinal direction (z) was restricted by the depth of the chamber (~700 nm). In this work, excitation was provided by a 638 nm laser (Obis, Coherent, Santa Clara, CA). The scanning pattern was chosen to be a 32-point "knight's tour" (33) (dwell time: 600 ns per point), which covers an area of ~3 μm × 3 μm at the sample plane. The focused beam waist ($1/e^2$) was ~0.75 μm. The laser power at the back aperture of the objective was ~40 μW, which resulted in an average illumination intensity of ~500 Wcm^{-2} at the sample (with beam scanning). For more details on the ABEL trap excitation and detection optics, see the legend for Fig. S2.

The microfluidic sample chamber was custom made in Princeton University's nanofabrication facility on ultraviolet-grade fused silica wafers and passivated with polyethylene glycol (PEG) (35). Specifically, after Piranha cleaning (3:1 mixture of sulfuric acid and hydrogen peroxide) and ~3 min sonication (or ~15 min incubation) in 1 M potassium hydroxide, the trapping chambers were incubated in a solution containing 500 mg mPEG-silane (MW: 5 kDa; Laysan Bio, Arab, AL), 10 mL ethanol, 250 μL water, and 50 μL acetic acid (10 mM). The PEGylation reaction was allowed to proceed at room temperature for at least 48 h in the dark. Before the experiment, the chamber was pretreated with 0.5% Tween 20 in HN100 buffer (pH 7.5) (36) and rinsed extensively with ultrapure water.

Single-molecule diffusometry

The diffusion coefficient (D) of a trapped single molecule was estimated using a maximal likelihood approach developed previously (30). Briefly, the residual motion of a single molecule in the trap consists of (uncompensated) diffusion and voltage-induced electrokinetic drifts. Analysis of the motion trajectory with a recorded history of voltage inputs yields single-molecule motion parameters (both the diffusion coefficient D and the electrokinetic mobility). Because the photon-by-photon position tracking entails a high degree of localization uncertainty, an expectation-maximization framework was developed to iteratively achieve accurate position trajectory reconstruction and parameter estimation.

Data analysis

All data analysis was performed using customized software written in MATLAB (The MathWorks, Natick, MA). First, the raw arrival times of fluorescence photons were binned at 5 ms to identify regions that correspond to individual molecules. An intensity change point algorithm (37) was applied to aid data segmentation. We used the following rules to identify the start and end times of a single molecule: 1) a brightness change from background to a stable high level is the beginning of a single-molecule event; 2) a brightness change from a stable high level to background is the termination of a single-molecule event; and 3) a transient brightness spike is the signature of a second molecule diffusing into the trap and data immediately after the spike is assigned to a new molecule. After segmentation, brightness and diffusivity values associated with a single molecule were averaged and processed further.

RESULTS

A focus lock improves single-molecule diffusometry stability

To differentiate molecular complexes by their hydrodynamic size, it is important to measure single-molecule diffusion coefficient (D) precisely and reproducibly. We accomplish this by using an ABEL trap to capture the molecule of interest in solution, allowing its diffusive motion to be continuously observed over many seconds. From statistical analysis of the residual in-trap motion, D of a single molecule can be extracted with high precision (30). We have previously shown that uncertainty in D measured with the ABEL trap scales with $1/\sqrt{N}$ (N, the number of photons detected from the single molecule, Fig. S1). However, focus drift during recording can prevent the photon-limited precision from being reached because defocus leads to a larger scanning beam at the trapping plane, which deteriorates the accuracy of the D estimation algorithm (lateral drifts, on the other hand, do not significantly affect D estimation). The extent of the focus drift is often variable between experiments, affecting the diffusometry measurements to varying degrees. To counteract focus drift and thus improve D estimation, we implemented a focus lock system similar to many other microscopy platforms (38–41). In this approach, an auxiliary laser is reflected off the coverslip-sample interface, and the position of the reflection spot on a camera, which is sensitive to the objective-sample distance, is used as a setpoint for z-piezo stage feedback (Figs. 2 *A* and S2). Our system achieved a focus stability of ~8 nm (SD, Fig. 2 *B*) and effectively eliminated defocus-induced drift in diffusion estimation (Fig. 2, *C* and *D*). With the focus locked, we achieved near photon-limited precision in D estimation over hour-long experiments ($\frac{\mathrm{std}(D)}{\overline{D}} = 0.05$, for D~50 $\mu m^2/s$ with 1 s measurement time, Fig. S1).

Diffusion contrast maps single-molecule DNA-protein interactions with and without PIFE

To demonstrate the application of diffusion contrast measurements to DNA-protein interactions, we first designed an experiment to cross-validate our approach with PIFE. We measured a 15-bp duplex DNA construct with a *Bam*HI binding site (GGATCC) (Table S1) with and without *Bam*HI in solution. With Ca^{2+} in place of Mg^{2+} in our buffer solution, *Bam*HI is expected to bind stably at the recognition sequence without inducing DNA cleavage (42). The DNA substrate is fluorescently labeled with a Cy5 dye at the terminal base, and the separation between Cy5 and the binding site is two base-pairs. Previously, it was demonstrated that at such a small distance, Cy5 displays a robust PIFE response (17). As a result, in our experiment, specific binding of *Bam*HI is expected to lower the diffusion coefficient of the DNA and simultaneously increase Cy5 brightness.

Without *Bam*HI, individual DNA duplexes (Fig. 3 *A*, top) showed homogenous brightness (~110 cnts/5 ms) and

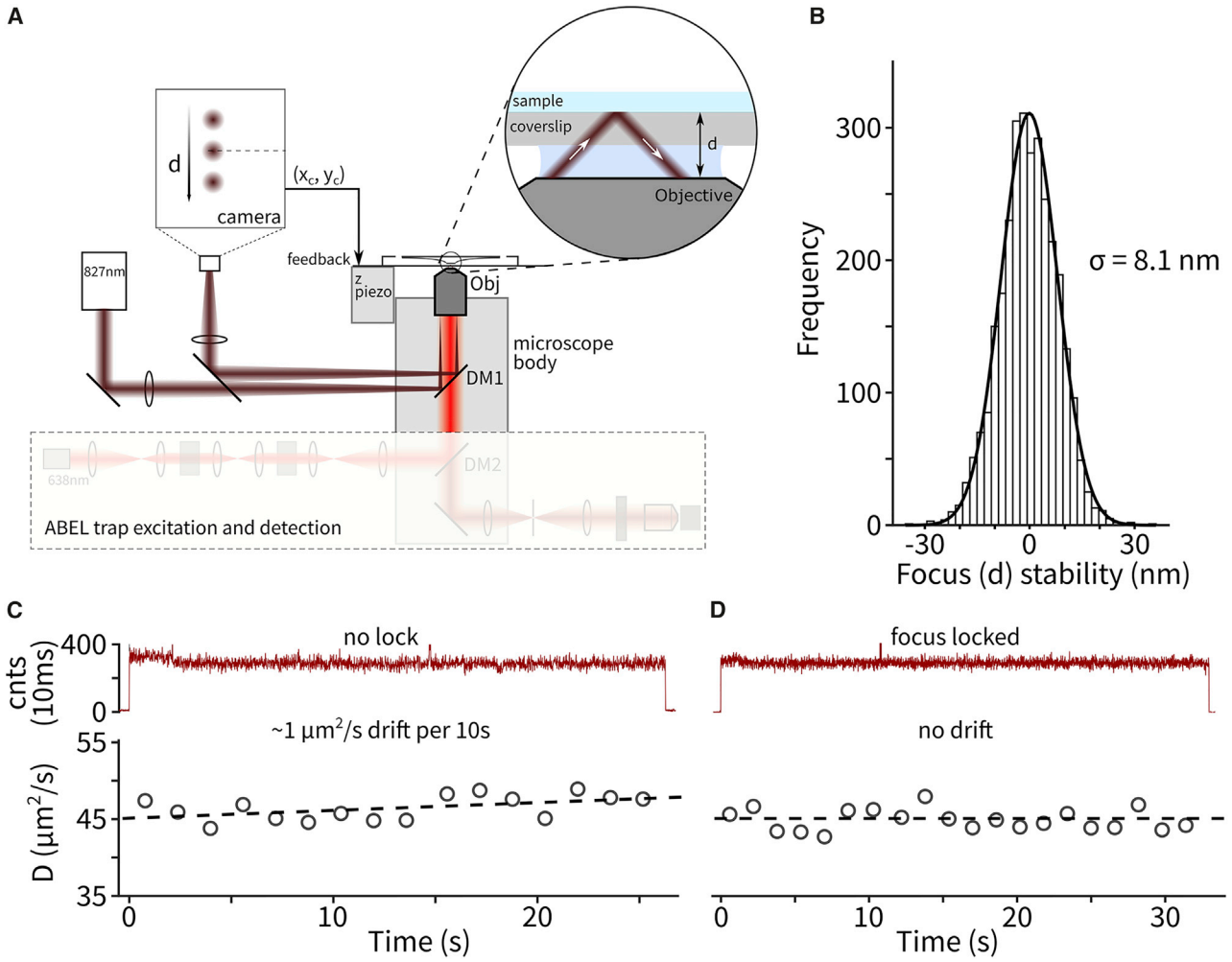

FIGURE 2 A focus lock system improves single-molecule *D* estimation. (*A*) Simplified schematic of the focus lock design. A near-infrared laser is reflected off the coverslip and imaged on to a camera. Changes in the objective-sample distance (d) result in lateral position (x_c and y_c) shifts of the camera spot. The difference between the spot position and a user-provided setpoint is used as the error signal for focus stabilization. (*B*) A representative distribution of deviations of the objective-sample distance (d) from the setpoint when the focus lock is engaged. The SD (σ) is extracted by a Gaussian fit. (*C*) An example trapping trace recorded with severe focus drift. Top: brightness in 10-ms bins. Bottom: estimated diffusion coefficient every 1.4 s. The apparent increase of diffusion coefficient is an artifact due to the excitation beam drifting out of focus. The dashed line is a linear fit of the data. (*D*) A representative trace recorded with the focus locked. The measured diffusion coefficient remains stable over time.

diffusion coefficient (~115 $\mu m^2/s$) (Fig. 3 *A*, *bottom*). When the measurement was conducted in the presence of 10 nM *Bam*HI (with Ca^{2+} in place of Mg^{2+} to prevent DNA cleavage), two different populations were seen (Fig. 3 *B*). One population was evidently the bare DNA as its brightness and diffusivity values closely resembled those observed in the DNA only measurement. The other population displayed the behavior expected from specifically bound *Bam*HI-DNA complexes: a higher brightness (~182 cnts/5 ms) because of PIFE and a lower diffusion coefficient (~68 $\mu m^2/s$). Further, this high-brightness, low-*D*-population decreased in abundance when a 10-fold lower concentration (1 nM) of *Bam*HI was used (Fig. S3) and was not observed in control experiments with mutant DNA (containing a single base change in the recognition sequence, Fig. S4 *A*) or a noncognate protein (*Eco*RI, Fig. S4 *B*). We observed a fluorescence enhancement factor of 1.65-fold, consistent with previous measurements (15) (1.9-fold enhancement at 1 bp away). In addition, the measured diffusion coefficient of the *Bam*HI-DNA complex (~68 $\mu m^2/s$) agrees with structure guided modeling (see Modeling the diffusion coefficient of DNA-protein complexes using extHullRad). Importantly, all molecules identified as *Bam*HI-DNA complexes by diffusivity contrast displayed enhanced brightness, demonstrating excellent consistency of both modalities in this example. Nevertheless, a small fraction of the *Bam*HI-bound complex showed lower

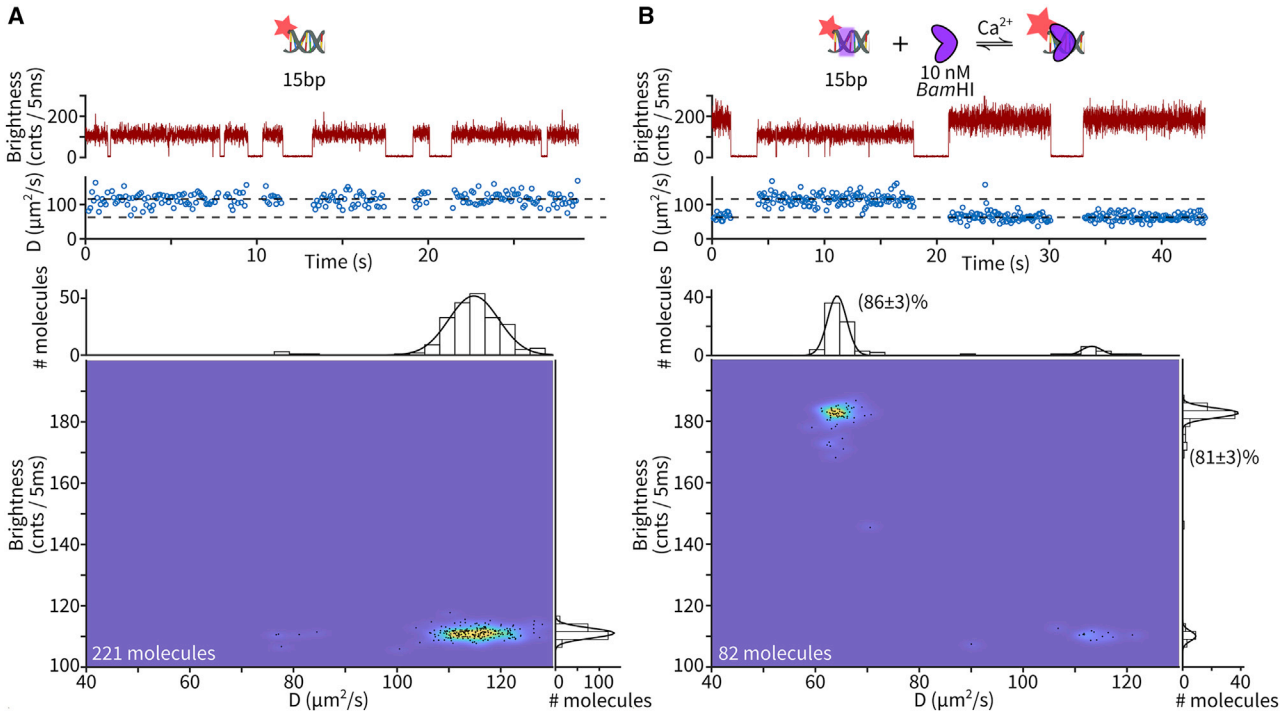

FIGURE 3 Probing *Bam*HI binding to 15-bp duplex DNA using PIFE and diffusivity contrast. (*A*) DNA without *Bam*HI. Top: representative time trace showing single-molecule brightness (5-ms bins) and measured diffusivity (every 100 ms) Bottom: *D*-brightness scatter plot of 221 measured molecules. Every black dot represents the diffusivity and brightness of a single molecule averaged over the trapping period. The underlying density is estimated using a two-dimensional (2D) kernel density estimator. Marginal histograms are fit with a single-component Gaussian function (fitted mean: 114.8 $\mu m^2/s$, SD: 3.4 $\mu m^2/s$). (*B*) DNA with 10 nM *Bam*HI. Top: representative time trace showing single-molecule brightness (5-ms bins) and measured diffusivity (every 100 ms). Bottom: *D*-brightness scatter plot of 82 molecules. Both marginal histograms are fit with a two-component Gaussian function, and the relative abundance of the major population is extracted from the fit.

fluorescence enhancement. We speculate that this could be due to heterogeneity in Cy5's photophysical behavior or *Bam*HI's binding geometry.

We next measured DNA-protein binding without PIFE. We used a Cy5-labeled, 40-bp duplex DNA with an *Eco*RI binding site (GAATTC) 27 basepairs away from the terminal Cy5. Previous work suggested that PIFE should not be detectable at this separation (15). Indeed, when we probed the DNA substrates molecule-by-molecule in the presence of 1 nM *Eco*RI, we observed homogeneous brightness among the molecules probed (Fig. 4, *top*). The diffusion coefficient, on the other hand, displayed two distinct levels that correspond to bare and *Eco*RI-bound DNA (Fig. 4), respectively. (A minor population with *D* $\sim$95 $\mu m^2/s$ and brightness $\sim$110 cnts/5 ms was also observed and identified as unhybridized, Cy5-labeled, single-strand DNA.) Note that in this example, conventional single-molecule fluorescence microscopy, which records only fluorescence brightness, would not be able to differentiate bound and unbound DNA molecules. Diffusivity contrast, on the other hand, provides a general and reliable mapping of DNA-protein interactions.

Modeling the diffusion coefficient of DNA-protein complexes using extHullRad

We next developed a modeling pipeline to associate measured diffusivity values with particular DNA-protein complexes. Predicting the diffusion coefficient of biological macromolecules from atomic coordinates is well established (43), and many accessible and easy-to-use tools (31,44) are available. However, these modeling tools cannot be directly applied to the samples in our experiments because of the lack of atomic structures for our full DNA-protein complexes (available database structures of DNA-binding proteins are often determined with very short or no substrate DNA). Inspired by the recently developed HullRad framework (31), we recognize that without full structural data, the hydrodynamic properties of DNA-protein assemblies can still be modeled by a composite approach based on constructing the smallest envelope (convex hull) that encompasses the entire complex in three dimensions. Our pipeline ("extHullrad," Fig. 5 *A*) starts with an existing protein-DNA structure. The DNA portion is replaced with a cylindrical rod (radius of 1 nm and 0.34 nm rise per basepair), aligned to the

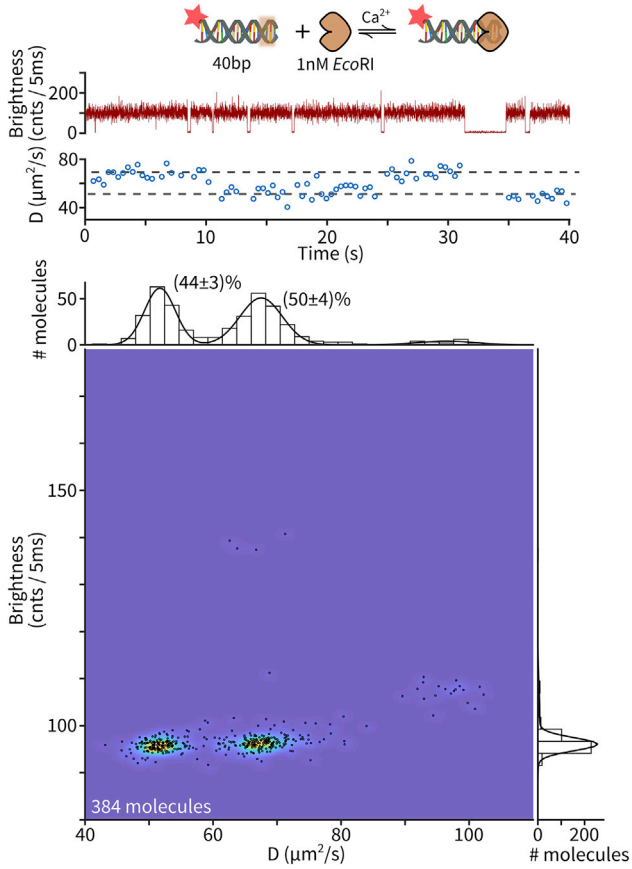

FIGURE 4 Diffusivity contrast maps *Eco*RI-DNA interactions without PIFE. Top: representative time trace showing single-molecule brightness (5-ms bins) and measured diffusivity (every 100 ms) Bottom: *D*-brightness scatter plot of 384 measured molecules. Every black dot represents the diffusivity and brightness of a single molecule averaged over the trapping period. The underlying density is estimated using a 2D kernel density estimator. The marginal histogram along the brightness axis is fit with a single-component Gaussian function, whereas the marginal histogram along the diffusivity axis is fit with a three-component Gaussian function. The relative abundance of the two major populations are extracted from the fit.

DNA axis and binding site in the original structure. This allows duplexes of different lengths (much shorter than the 40–50 nm persistence length of double-stranded DNA (dsDNA) (45,46)) to be modeled without molecular details. The combined set of protein atomic coordinates and calculated DNA coordinates is then used as the input to the original HullRad algorithm (31) (Fig. 5 *A*, *inner square*), in which the convex hull and hydration shell around a molecular complex is approximated as a prolate ellipsoid, and an extension of the Stokes-Einstein equation is used to calculate the translational diffusion coefficient (see (31) for details). The extHullRad routine is implemented in Python and available as Supporting code.

In Fig. 5 *B*, we compare the modeling results to single-molecule diffusometry measurements. We first confirm that measured *D* values of bare DNA (15, 24, 31, 40, and 52 bp) agree with HullRad modeling (Fig. 5 *B*, *orange circles*). We then compare measurements of two different proteins (*Bam*HI and *Eco*RI) bound to substrate dsDNA of different lengths (15–52 bp, nine datasets in total, Figs. S5–S9). For each condition, we use the exHullRad pipeline to model the diffusion coefficient of the DNA-protein complex (starting from Protein Data Bank, PDB: 2BAM for *Bam*HI and PDB: 1ERI for *Eco*RI) and compare to experimental results (Figs. S5–S9). We achieved satisfactory agreement between the modeled and measured *D* values of the complexes (a mean error of 5.2% across nine complexes, Fig. 5 *B*, *triangles*). Importantly, it is critical to model the shape of the DNA-protein complexes used here, a task that extHullRad was designed to accomplish. A naive prediction that assumes complexes are spherical and uses $D \propto \mathrm{MW}^{-1/3}$ scaling produced much larger discrepancies (Fig. 5 *B*, *diamonds*).

Diffusion contrast with PIFE probes ternary complexes with sequence context

Finally, we demonstrate that combining diffusivity contrast and PIFE enables three-component DNA-protein reactions to be resolved at the single-molecule level. We used a 40-bp DNA duplex with both *Bam*HI and *Eco*RI binding sites and aimed to identify all possible binding configurations in the presence of the two restriction enzymes (Fig. 6 *A*). As above, the PIFE-sensitive dye Cy5 is placed 2 bp away from the *Bam*HI site and 27 bp away from the *Eco*RI site. We anticipated that PIFE would report the occupancy of the *Bam*HI site, and diffusivity would probe the number of protein molecules bound (i.e., 0, 1, and 2), thus giving rise to four distinct populations in the *D*-brightness space (Fig. 6 *B*). Experiments at several concentrations of *Eco*RI confirmed this pattern with four populations clearly visible (Fig. 6, *C* and *D*). The two populations at lower brightness (~95 cnts/5 ms), one with *D* around 67 $\mu m^2/s$ and the other with *D* ~53 $\mu m^2/s$, can be assigned as unbound DNA and DNA-*Eco*RI complex, respectively, based on the absence of PIFE and comparison to data shown in Fig. S8 (DNA only and DNA with one restriction enzyme each). The two populations at higher brightness (160 cnts/5 ms) have *Bam*HI bound. Among these, the *D* ~53 $\mu m^2/s$ population is the DNA-*Bam*HI binary complex based on a similar *D* to DNA-*Eco*RI and comparison to Fig. S8 *B*. Finally, the population with the lowest *D* (~45 $\mu m^2/s$) can be assigned to the fully assembled ternary complex (DNA-*Bam*HI-*Eco*RI) based on the high brightness and the larger hydrodynamic size compared with DNA-*Bam*HI. Furthermore, the relative abundance of the populations shifted as the *Eco*RI

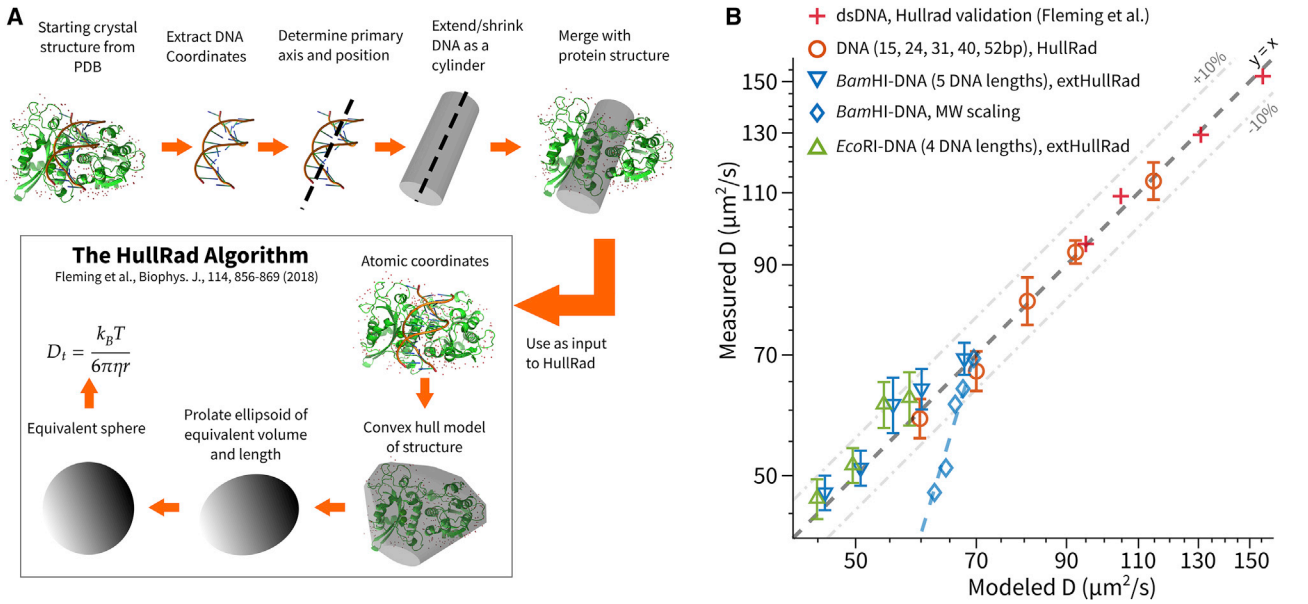

FIGURE 5 extHullRad successfully predicts the diffusion coefficient of DNA-protein complexes. (*A*) Workflow of extHullRad (see text for details). (*B*) Comparison of modeled and measured diffusivity values across different samples. Red plus signs: short duplex DNA molecules (reproduced from (31)) that were used to validate the modeling accuracy of the original HullRad framework. Orange circles: DNA molecules from this study (15, 24, 31, 40, and 52 bp) measured using focus-stabilized single-molecule diffusometry and modeled using HullRad. Blue triangles: *Bam*HI-bound 15, 24, 31, 40, and 52 bp dsDNA, measured in this work and modeled using extHullRad. Green triangles: *Eco*RI-bound 24, 31, 40, 52 bp dsDNA, measured in this work and modeled using extHullRad. Blue diamonds: comparison of the measured D of *Bam*HI-DNA complexes with a naive molecular weight scaling *D* prediction model ($D \propto MW^{-1/3}$). Error bars of measured *D* represent SD values from Gaussian fits of *D* histograms (Figs. S5–S9).

concentration was varied from 0.4 to 2 nM (Figs. 6, *C* and *D* and S10), in a way that is consistent with the expected *Eco*RI binding site occupancy of each state in our assignment. Note that in this example, neither the PIFE signal nor the diffusion coefficient alone would be able to resolve all binding configurations.

DISCUSSION

This work establishes single-molecule diffusivity as a general readout to probe DNA-protein interactions in solution. In contrast to many classic biochemical approaches for analyzing protein-nucleic acid interactions (e.g., the electrophoretic mobility shift assay (47), which separates molecular complexes into distinct gel bands), the method presented here operates on individual molecules in solution at chemical equilibrium. From analyzing the relative abundance of the protein-bound and free DNA species, we estimated a K_d of ∼2–5 nM for *Bam*HI and ∼1 nM for *Eco*RI (Fig. S11) under the buffer condition (20 mM HEPES (pH 7.8) with 25 mM NaCl and 2 mM $CaCl_2$) and sequence contexts used in this study. These values are in line with recent solution phase experiments using fluorescence anisotropy (K_d ∼9 nM for *Bam*HI with Ca^{2+}) (48) but larger than values measured previously using a filter binding assay (42) (K_d ∼0.2 nM for *Bam*HI) and a mobility shift assay (49) (K_d ∼0.4 nM for *Eco*RI without Ca^{2+}). The discrepancy may be due to differences in assay medium, sequence context, or the influence of a fluorophore close to the binding site. Beyond an equilibrium measurement of binding affinity, observing single complexes under equilibrium also offers a window into the dynamics and heterogeneity of protein-nucleic acid interactions (Fig. S12). Information on the kinetics and relative order of binding steps may shed new light on the favored pathways of protein-nucleic acid assembly.

Measurements of equilibrium binding in solution are also possible using fluorescence anisotropy (50,51), which detects binding through the resulting slower rotational diffusion of the DNA-protein complex. Compared with translational diffusivity, rotational diffusion is more sensitive to binding, but anisotropy measurements are often complicated by the rotational flexibility of the dye label itself. Our approach based on direct measurements of translational diffusion is not affected by linker motions of the fluorescent label.

At the single-molecule level, diffusivity contrast provides an alternative to PIFE for sensing the binding between labeled nucleic acid and unlabeled protein. Using a specially designed DNA substrate, we have verified that both methods reliably identify protein

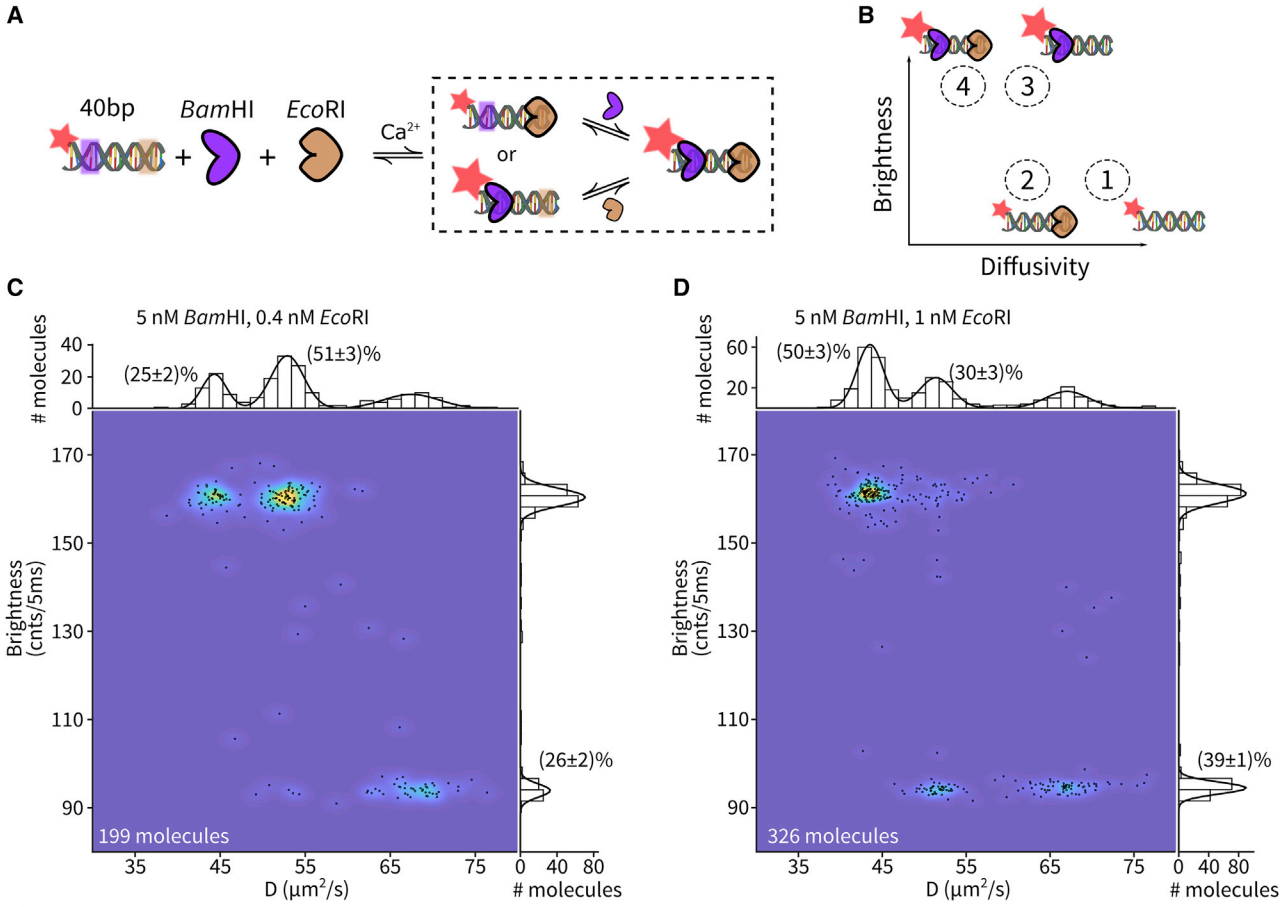

FIGURE 6 Combining single-molecule diffusivity contrast and PIFE identifies all four binding configurations between a dual binding site DNA and two proteins. (*A*) Experimental design: a 40 bp DNA containing both *Bam*HI and *Eco*RI binding sites can undergo sequential binding to arrive at the DNA-*Bam*HI-*Eco*RI ternary complex. (*B*) Four possible binding configurations are possible in solution and can be resolved in the *D*-brightness parameter space. (*C*) Experimental *D*-brightness scatter plot of 199 measured molecules with 5 nM *Bam*HI and 0.4 nM *Eco*RI. (*D*) Experimental *D*-brightness scatter plot of 326 measured molecules with 5 nM *Bam*HI and 1 nM *Eco*RI. In (*C* and *D*), every black dot represents the diffusivity and brightness of a single molecule averaged over the trapping period. The underlying density is estimated using a 2D kernel density estimator. The marginal histogram along the brightness axis is fit with a two-component Gaussian function, whereas the marginal histogram along the diffusivity axis is fit with a three-component Gaussian function. The relative abundance of the populations is extracted from the respective fits.

binding. Each modality has its advantages and disadvantages. PIFE is straightforward to implement on existing single-molecule fluorescence platforms but requires strategically placing a sensor dye within a few nanometers of the binding site. Furthermore, only a limited selection of dyes (mostly cyanine) are PIFE sensitive, although other dyes sensitive to their microenvironment, such as twisted intramolecular charge transfer fluorophores (52), might provide further options for experimental design. Diffusivity contrast requires sophisticated hardware and analysis algorithms to implement but relaxes design constraints associated with PIFE. There is no restriction on dye type or labeling location on the nucleic acid. Importantly, PIFE is a photophysical phenomenon, and combining with other spectroscopic modalities (e.g., single-molecule Förster resonance energy transfer) often results in compounded signals requiring sophisticated analysis and experimental design to delineate (53,54). Stacking of cyanine dyes at the end of DNA duplexes (55) as well as protein-dye orientation (56) can also complicate the interpretation of PIFE signals (57). Diffusivity contrast, on the other hand, is based on a physical property of molecular complexes (i.e., hydrodynamic size) and is completely orthogonal to spectroscopic readouts. Combining diffusivity contrast with other spectroscopic readouts adds an extra dimension (35) that enhances single-molecule measurements. Moreover, we showed that diffusivity contrast provides complex-level structural information through the extHullRad modeling framework. Meanwhile, the time resolution of PIFE

(<10 ms) is much higher than our current implementation of diffusivity measurement (~200 ms), making PIFE a more suitable method to probe rapid binding/unbinding events.

Given the complementary nature of PIFE and diffusivity contrast, combining the two modalities brings new capabilities. We have demonstrated simultaneous mapping of stoichiometry ("how many protein molecules are bound") and sequence context ("where are they bound") in the interactions between one DNA substrate and two proteins. Similar ideas can be used to differentiate specific and nonspecific binding. We envision that these capabilities will enable new single-molecule measurements of many fascinating phenomena in protein-nucleic acid interactions, for example target search (58) and DNA allostery (59).

SUPPORTING MATERIAL

Supporting material can be found online at https://doi.org/10.1016/j.bpr.2021.100009.

AUTHOR CONTRIBUTIONS

H.W., M.L., and Q.W. designed the research. H.W. and Q.W. performed the experiments and analyzed the data. M.L. developed the extHullRad framework.

ACKNOWLEDGMENTS

We thank Haw Yang and his lab for feedback and suggestions, Patrick Fleming for discussion of the extHullRad framework, and New England BioLabs customer support for providing concentration values of their *Bam*HI and *Eco*RI products.

This work is funded by the Lewis-Sigler Fellowship to Q.W. and the U.S. Department of Energy Office of Basic Energy Sciences and Photosynthetic Systems grant DE-SC0002423.

DECLARATION OF INTERESTS

The authors declare no competing interests.

REFERENCES

1. Ha, T., A. G. Kozlov, and T. M. Lohman. 2012. Single-molecule views of protein movement on single-stranded DNA. *Annu. Rev. Biophys.* 41:295–319.
2. Bell, J. C., and S. C. Kowalczykowski. 2016. Mechanics and single-molecule interrogation of DNA recombination. *Annu. Rev. Biochem.* 85:193–226.
3. Michaelis, J., and B. Treutlein. 2013. Single-molecule studies of RNA polymerases. *Chem. Rev.* 113:8377–8399.
4. Finkelstein, I. J., and E. C. Greene. 2013. Molecular traffic jams on DNA. *Annu. Rev. Biophys.* 42:241–263.
5. Mohapatra, S., C.-T. Lin, …, T. Ha. 2020. Single-molecule analysis and engineering of DNA motors. *Chem. Rev.* 120:36–78.
6. Candelli, A., M. Modesti, …, G. J. L. Wuite. 2013. Single-molecule views on homologous recombination. *Q. Rev. Biophys.* 46:323–348.
7. Hoskins, A. A., J. Gelles, and M. J. Moore. 2011. New insights into the spliceosome by single molecule fluorescence microscopy. *Curr. Opin. Chem. Biol.* 15:864–870.
8. Friedman, L. J., and J. Gelles. 2012. Mechanism of transcription initiation at an activator-dependent promoter defined by single-molecule observation. *Cell.* 148:679–689.
9. Collins, B. E., L. F. Ye, …, E. C. Greene. 2014. DNA curtains: novel tools for imaging protein-nucleic acid interactions at the single-molecule level. *In* Methods in Cell Biology, *Vol. 123*. Academic Press Inc., pp. 217–234.
10. Christian, T. D., L. J. Romano, and D. Rueda. 2009. Single-molecule measurements of synthesis by DNA polymerase with base-pair resolution. *Proc. Natl. Acad. Sci. USA.* 106:21109–21114.
11. Feng, X. A., M. F. Poyton, and T. Ha. 2021. Multicolor single-molecule FRET for DNA and RNA processes. *Curr. Opin. Struct. Biol.* 70:26–33.
12. Holzmeister, P., G. P. Acuna, …, P. Tinnefeld. 2014. Breaking the concentration limit of optical single-molecule detection. *Chem. Soc. Rev.* 43:1014–1028.
13. van Oijen, A. M. 2011. Single-molecule approaches to characterizing kinetics of biomolecular interactions. *Curr. Opin. Biotechnol.* 22:75–80.
14. Luo, G., M. Wang, …, X. S. Xie. 2007. Single-molecule and ensemble fluorescence assays for a functionally important conformational change in T7 DNA polymerase. *Proc. Natl. Acad. Sci. USA.* 104:12610–12615.
15. Hwang, H., H. Kim, and S. Myong. 2011. Protein induced fluorescence enhancement as a single molecule assay with short distance sensitivity. *Proc. Natl. Acad. Sci. USA.* 108:7414–7418.
16. Hwang, H., and S. Myong. 2014. Protein induced fluorescence enhancement (PIFE) for probing protein-nucleic acid interactions. *Chem. Soc. Rev.* 43:1221–1229.
17. Stennett, E. M. S., M. A. Ciuba, …, M. Levitus. 2015. Demystifying PIFE: the photophysics behind the protein-induced fluorescence enhancement phenomenon in Cy3. *J. Phys. Chem. Lett.* 6:1819–1823.
18. Song, D., T. G. W. Graham, and J. J. Loparo. 2016. A general approach to visualize protein binding and DNA conformation without protein labelling. *Nat. Commun.* 7:10976.
19. Markiewicz, R. P., K. B. Vrtis, …, L. J. Romano. 2012. Single-molecule microscopy reveals new insights into nucleotide selection by DNA polymerase I. *Nucleic Acids Res.* 40:7975–7984.
20. Luo, Y., J. A. North, …, M. G. Poirier. 2014. Nucleosomes accelerate transcription factor dissociation. *Nucleic Acids Res.* 42:3017–3027.
21. Myong, S., S. Cui, …, T. Ha. 2009. Cytosolic viral sensor RIG-I is a 5′-triphosphate-dependent translocase on double-stranded RNA. *Science.* 323:1070–1074.
22. Marko, R. A., H. W. Liu, …, G. Cosa. 2013. Binding kinetics and affinities of heterodimeric versus homodimeric HIV-1 reverse transcriptase on DNA-DNA substrates at the single-molecule level. *J. Phys. Chem. B.* 117:4560–4567.
23. Schuck, P. 2013. Analytical ultracentrifugation as a tool for studying protein interactions. *Biophys. Rev.* 5:159–171.
24. Schubert, F., H. Zettl, …, G. Krausch. 2003. Comparative thermodynamic analysis of DNA–protein interactions using surface plasmon resonance and fluorescence correlation spectroscopy. *Biochemistry.* 42:10288–10294.
25. Cristóvão, M., E. Sisamakis, …, P. Friedhoff. 2012. Single-molecule multiparameter fluorescence spectroscopy reveals directional MutS binding to mismatched bases in DNA. *Nucleic Acids Res.* 40:5448–5464.

26. Shen, H., L. J. Tauzin, …, C. F. Landes. 2017. Single particle tracking: from theory to biophysical applications. *Chem. Rev.* 117:7331–7376.
27. Low-Nam, S. T., K. A. Lidke, …, D. S. Lidke. 2011. ErbB1 dimerization is promoted by domain co-confinement and stabilized by ligand binding. *Nat. Struct. Mol. Biol.* 18:1244–1249.
28. Hansen, A. S., M. Woringer, …, X. Darzacq. 2018. Robust model-based analysis of single-particle tracking experiments with SpotOn. *eLife.* 7:e33125.
29. Spille, J. H., T. P. Kaminski, …, U. Kubitscheck. 2015. Direct observation of mobility state transitions in RNA trajectories by sensitive single molecule feedback tracking. *Nucleic Acids Res.* 43:e14.
30. Wang, Q., and W. E. Moerner. 2014. Single-molecule motions enable direct visualization of biomolecular interactions in solution. *Nat. Methods.* 11:555–558.
31. Fleming, P. J., and K. G. Fleming. 2018. HullRad: fast calculations of folded and disordered protein and nucleic acid hydrodynamic properties. *Biophys. J.* 114:856–869.
32. Rasnik, I., S. A. McKinney, and T. Ha. 2006. Nonblinking and long-lasting single-molecule fluorescence imaging. *Nat. Methods.* 3:891–893.
33. Wang, Q., and W. E. Moerner. 2011. An adaptive Anti-Brownian ELectrokinetic trap with real-time information on single-molecule diffusivity and mobility. *ACS Nano.* 5:5792–5799.
34. Wang, Q., and W. E. Moerner. 2010. Optimal strategy for trapping single fluorescent molecules in solution using the ABEL trap. *Appl. Phys. B.* 99:23–30.
35. Wilson, H., and Q. Wang. 2021. ABEL-FRET: tether-free single-molecule FRET with hydrodynamic profiling. *Nat. Methods.* 18:816–820.
36. Pan, H., Y. Xia, …, W. Wang. 2015. A simple procedure to improve the surface passivation for single molecule fluorescence studies. *Phys. Biol.* 12:045006.
37. Watkins, L. P., and H. Yang. 2005. Detection of intensity change points in time-resolved single-molecule measurements. *J. Phys. Chem. B.* 109:617–628.
38. Ortega Arroyo, J., D. Cole, and P. Kukura. 2016. Interferometric scattering microscopy and its combination with single-molecule fluorescence imaging. *Nat. Protoc.* 11:617–633.
39. Douglass, K. M., C. Sieben, …, S. Manley. 2016. Super-resolution imaging of multiple cells by optimised flat-field epi-illumination. *Nat. Photonics.* 10:705–708.
40. Balzarotti, F., Y. Eilers, …, S. W. Hell. 2017. Nanometer resolution imaging and tracking of fluorescent molecules with minimal photon fluxes. *Science.* 355:606–612.
41. Bellvé, K.. Pretty good focus. http://big.umassmed.edu/wiki/index.php/PgFocus.
42. Engler, L. E., P. Sapienza, …, L. Jen-Jacobson. 2001. The energetics of the interaction of BamHI endonuclease with its recognition site GGATCC. *J. Mol. Biol.* 307:619–636.
43. García de la Torre, J., and J. G. Hernández Cifre. 2020. Hydrodynamic properties of biomacromolecules and macromolecular complexes: concepts and methods. A tutorial mini-review. *J. Mol. Biol.* 432:2930–2948.
44. Ortega, A., D. Amorós, and J. García de la Torre. 2011. Prediction of hydrodynamic and other solution properties of rigid proteins from atomic- and residue-level models. *Biophys. J.* 101:892–898.
45. Hagerman, P. J. 1988. Flexibility of DNA. *Annu. Rev. Biophys. Biophys. Chem.* 17:265–286.
46. Baumann, C. G., S. B. Smith, …, C. Bustamante. 1997. Ionic effects on the elasticity of single DNA molecules. *Proc. Natl. Acad. Sci. USA.* 94:6185–6190.
47. Hellman, L. M., and M. G. Fried. 2007. Electrophoretic mobility shift assay (EMSA) for detecting protein-nucleic acid interactions. *Nat. Protoc.* 2:1849–1861.
48. Vanamee, É. S., H. Viadiu, …, A. K. Aggarwal. 2011. Asymmetric DNA recognition by the OkrAI endonuclease, an isoschizomer of BamHI. *Nucleic Acids Res.* 39:712–719.
49. Robinson, C. R., and S. G. Sligar. 1998. Changes in solvation during DNA binding and cleavage are critical to altered specificity of the EcoRI endonuclease. *Proc. Natl. Acad. Sci. USA.* 95:2186–2191.
50. Lakowicz, J. R. 2006. Principles of Fluorescence Spectroscopy. Springer Science, Berlin, Germany.
51. Yang, H.-Y., and W. E. Moerner. 2018. Resolving mixtures in solution by single-molecule rotational diffusivity. *Nano Lett.* 18:5279–5287.
52. Sasaki, S., G. P. C. Drummen, and G. Konishi. 2016. Recent advances in twisted intramolecular charge transfer (TICT) fluorescence and related phenomena in materials chemistry. *J. Mater. Chem. C Mater. Opt. Electron. Devices.* 4:2731–2743.
53. Lerner, E., E. Ploetz, …, S. Weiss. 2016. A quantitative theoretical framework for protein-induced fluorescence enhancement-Förster-type resonance energy transfer (PIFE-FRET). *J. Phys. Chem. B.* 120:6401–6410.
54. Gidi, Y., M. Götte, and G. Cosa. 2017. Conformational changes spanning angstroms to nanometers via a combined protein-induced fluorescence enhancement-Förster resonance energy transfer method. *J. Phys. Chem. B.* 121:2039–2048.
55. Iqbal, A., S. Arslan, …, D. M. Lilley. 2008. Orientation dependence in fluorescent energy transfer between Cy3 and Cy5 terminally attached to double-stranded nucleic acids. *Proc. Natl. Acad. Sci. USA.* 105:11176–11181.
56. Nguyen, B., M. A. Ciuba, …, T. M. Lohman. 2019. Protein environment and DNA orientation affect protein-induced Cy3 fluorescence enhancement. *Biophys. J.* 117:66–73.
57. Rashid, F., V. S. Raducanu, …, S. M. Hamdan. 2019. Initial state of DNA-Dye complex sets the stage for protein induced fluorescence modulation. *Nat. Commun.* 10:2104.
58. Halford, S. E., and J. F. Marko. 2004. How do site-specific DNA-binding proteins find their targets? *Nucleic Acids Res.* 32:3040–3052.
59. Kim, S., E. Broströmer, …, X. S. Xie. 2013. Probing allostery through DNA. *Science.* 339:816–819.